

A Comparative Study on the Influence of Ventilation on Weather- and Fire-Induced Stack Effect in the Elevator Shafts of a High-Rise Building

*Lin Xue**, Research Center of Fluid Machinery Engineering and Technology, Jiangsu University, Zhenjiang 212013, China; Shanghai Fire Research Institute of MPS, Shanghai 200032, China

Shouqi Yuan, Research Center of Fluid Machinery Engineering and Technology, Jiangsu University, Zhenjiang 212013, China

Qize He, Shanghai Fire Research Institute of MPS, Shanghai 200032, China; Mechanical Engineering, University of Texas at Austin, Austin, TX 78712, USA

Received: 21 January 2017/**Accepted:** 24 September 2017

Abstract. This work assessed the impact of ventilation on both weather- and fire-induced stack effect in an 18-story high-rise office building. Elevator shafts are considered the main route of vertical air movement. Pressure distribution induced by cold weather within the elevator shafts was calculated theoretically. Computational fluid dynamics simulations of fire in the same high-rise building under different ventilation conditions were carried out with a fire dynamics simulator. It was found that ventilation exerted a more complex impact on fire than the weather-induced stack effect. For the weather-induced stack effect, the ventilation condition of the building only affected the height of the neutral pressure plane; in fire situations, it did not only affect the height of the neutral pressure plane in a similar manner to the weather-induced stack effect, but also influenced temperature and pressure distributions in the elevator shafts. The smoke movement and the distributions of temperature and pressure in elevator shafts are also learned. The smoke movement in high rises experienced four typical stages after ignition. The ventilation condition of the fire floor influences gas flow into elevator shafts, while that of the upper floors impacts the smoke rise speed in vertical shafts. When the stack effect finally reaches steady state, the gas temperature in the shaft decreases exponentially with height. Based on this assumption, a theoretical model was presented to characterize the fire-induced stack effect in typical high rises. Results showed that the model successfully predicts the pressure distribution in high-rise buildings.

Keywords: Stack effect, High rise, Fire, Weather, Elevator shaft

* Correspondence should be addressed to: Lin Xue, E-mail: sfrixuelin@vip.sina.com



1. Introduction

China is currently undergoing a rapid urbanization process, which has resulted in the continuous construction of high-rise buildings in large cities to stack huge numbers of homes and offices into limited space. High buildings tend to experience more stack effect problems than lower counterparts. Specifically, stack effect was shown to affect multiple phenomena in high-rise buildings, including additional energy loss caused by airflow, extensive smoke spread in case of fire, and loud noise resulting from air flowing through the cracks [1].

Stack effect is initially a building design issue. The basic theoretical analysis of stack effect is well known [2]. The pressure difference throughout a building is related to its temperature and elevation, as expressed by the following equation:

$$\Delta P = K_s \left(\frac{1}{T_0} - \frac{1}{T_l} \right) h, \quad (1)$$

where $K_s = 3460$ is a coefficient, T_0 and T_l are the environmental (exterior) and local (interior) temperatures, respectively, and h is the elevation. In cold weather, the normal outside–inside temperature difference induces stack effect in buildings. With respect to such weather-induced stack effect, previous investigations focused on actual pressure profiles [3, 4] and possible solutions to stack effect-related problems [5–8]. Nevertheless, stack effect is also a safety issue. In the particular case of fire taking place in a high-rise building, the air inside the building is heated, leading to stack effect. Because of the heat and mass transfer processes as a result of fire, coupled with heat loss from the walls, fire-induced stack effect is more complex than the one associated with weather. Cannon and Zukoski [9] studied the turbulent mixing in one closed shaft and developed one relationship between smoke rise time and the ratio of initial density difference between fluids inside and outside of the shaft. Water/saltwater experiments were conducted to verify the model. Tanaka et al. [10] conducted experiments to investigate the rise time of fire-induced buoyant plumes in the free space and in vertical shafts. Sun et al. [11, 12] assessed the movement of smoke in the stairwell of a full-scale six-story building experimentally and numerically. The smoke was induced by fire in an adjacent compartment. They found that the temperature of smoke in the stairwell generally decreases exponentially with height. Ji further investigated the smoke rise in a stairwell using the same facility [13, 14]. A network model was developed by Black [16] to predict the movement of smoke in elevator shafts. An improved zone model of smoke movement was introduced by Cooper [17] and partially verified by saltwater experiments. These models have been applied extensively [18]. However, studies using the CFD method to assess how smoke spreads through the elevator shafts of buildings are scarce. Meanwhile, this method is becoming a standard tool for fire hazard analysis and fire safety design of buildings.

Ventilation is one of the key factors that affects air flow in and out of a building. Jacques [19] and Koo et al. [20] evaluated weather-induced flow in high-rise buildings and identified the airtightness of architectural elements that comprise a

building as an important parameter minimizing stack effect problems. In addition, the spread of fire in a high-rise building is also restricted by compartmentalization, which involves dividing the building into discrete compartments, a process which hinders fire from spreading from one compartment to another. The configuration of the doors and windows of various compartments significantly affects the spread of smoke throughout the building [21, 22]. In this regard, Cheung et al. [23] simulated smoke spread from one room to another and found that the height of the door gaps has a significant effect on pressure and temperature distributions, which are important in controlling the spread of smoke. An efficient way to solve problems associated with the stack effect is to improve the overall airtightness of the whole building. However, separation failure between the different compartments within a high-rise building is inevitable. Therefore, the impact of ventilation on stack effect in high-rise buildings needs to be addressed.

In this study, the weather- and fire-induced stack effect in a typical 18-story high-rise office building was assessed theoretically and numerically. Elevator shafts are considered the main route of vertical air movement. Stack effect under different ventilation conditions, including changing the configurations of envelope windows and elevator doors, was comparatively evaluated. Results showed marked differences in ventilation effects between weather- and fire-induced stack effects.

2. Building Models

2.1. The Building

This study evaluated a typical 18-story high-rise office building (Fig. 1). The building model was simplified using the layout of the Chicago Committee on High Rise Buildings' (CCHRB) Office Research Tower. It is a hypothetical building designed to comply with building codes [mainly NFPA 101 (National Fire Protection Association 2012) and International Building Code 2012 (International Code Council 2012)]. This layout has been adopted for research on high-rise building evacuation.

The dimensions of the entire building were 43.0 m (W) \times 65.0 m (L) \times 80.0 m (H). The floor-to-floor height was 4.0 m except for the lobby at ground level, which had a floor-to-floor height of 12.0 m. An inner service core, with a dimension of 12.0 m \times 42.0 m, was located in the center of the building. The core was built for facilities and services needed in the building, including HVAC installations, elevator systems, stairs, storage rooms, and toilets. The service core was enclosed by shear walls except for the elevator lobbies. There were a total of eight elevators connecting all the stories of the building.

2.2. Flow Paths

Buildings are usually not hermetically sealed. There are a number of flow paths through both the exterior and interior walls. These flow paths consisted of the following: (1) leakages around the building envelope, (2) gaps around internal and elevator doors, and (3) office area and vertical shafts, e.g., elevator and stair

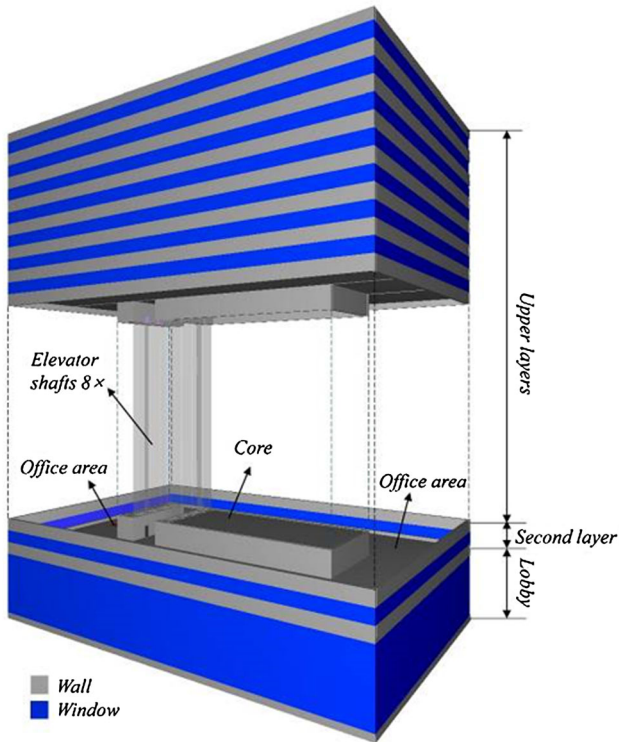


Figure 1. Structure of the building model.

shafts. It is noteworthy that the shapes and areas of a flow path may vary from one building to another, and more than one vertical shaft and internal door may exist along the path. In this research, we considered the most representative situation among the above three flow paths.

Of these, the most important flow path affecting smoke spread through elevator shafts to other levels includes the gaps around the elevator doors. In Klote's research [15], an area of roughly 0.047 m^2 of elevator door leakage was indicated. We surveyed the leakage areas of actual passenger elevator and stair doors in a typical office building (Fig. 2). The dimensions of the elevator door were 42 by 84 inches. Gaps were not only found at the centerline of the door, but also along the edges. The gaps were approximately $3/16$ inches wide (Fig. 2). Thus, the total area of these gaps was about 63.0 square inches (0.041 m^2). This value is very close to the leakage area in Klote's research. As a conservative consideration, 0.05 m^2 was used as the leakage area of a single elevator door in this research.

According to the survey, the stair door was sealed more efficiently than the elevator one. As shown in Fig. 2, due to the presence of a gate groove, there was hardly any gap around the stair door, except for the bottom frame. Thus, leakages through stair doors were much smaller than those through elevator doors. By

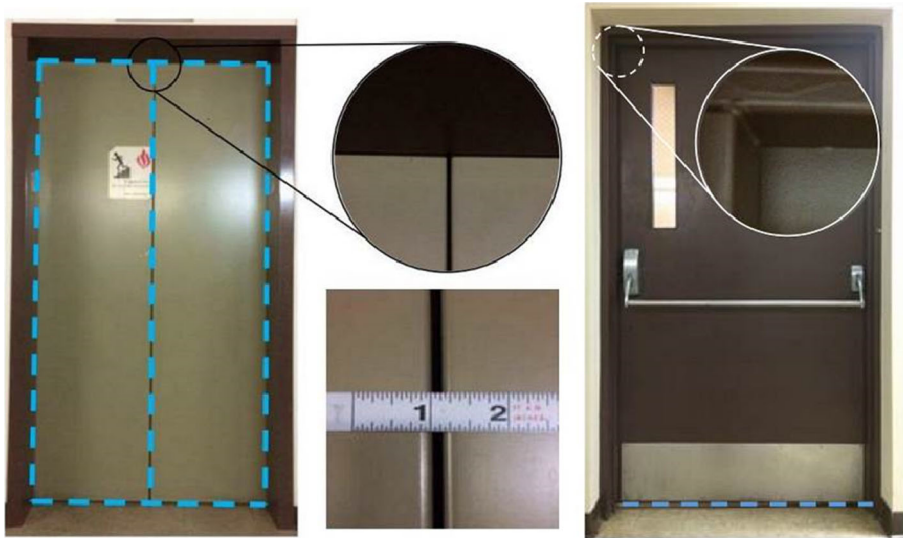


Figure 2. Locations of leakage areas for typical passenger elevator (left) and stair (right) doors in office buildings.

way of simplification, smoke spread was assumed to occur only through the elevator shafts in this study.

Leakages are also found in the building envelope. According to the ASHRAE Handbook, the leakage area of exterior walls should be about $0.002 \text{ in}^2/\text{ft}^2$, with a flow coefficient of about 0.65. Thus, the calculated leakage area of exterior walls per floor is $A_w = 4 \times 2 \times (63 + 43) \times 0.00014 = 0.12 \text{ m}^2$ for the upper floors, and $A_w = 12 \times 2 \times (63 + 43) \times 0.00014 = 0.36 \text{ m}^2$ for the lobby floor. The exterior leakage area of any given floor of the building is quite small, which indicates that most buildings are well-enclosed nowadays.

For the sizes of other leakages along the flow paths, we referred to the recommended values of the NFPA standard for smoke control systems. The values listed in Table 1 are representative leakage areas commonly found in office buildings and were deemed suitable for the characterization of smoke spread characteristics [24, 25].

Elevator cars in the shafts might have a significant effect on smoke spread in the building. The presence of cars reduces the sectional area of the shafts, as well as the rate at which smoke spreads. According to current codes, elevators should not normally be used in a situation of fire outbreak. All cars should be recalled to the ground floor during fire, which activates a detector in the elevator lobby. In this study, the elevator shafts were simplified and modeled as being empty. This situation has a similar effect to moving all the elevator cars to the lobby floor.

Table 1
Summary of Flow Paths

Component	Area (m ²)	References
Exterior wall of upper layers	0.12	–
Exterior wall of lobby	0.36	–
Open window	Perimeter × 2 (2 m in height)	–
Interior single door	1.9	[24, 25]
Interior double door	3.9	[24, 25]
Closed interior single door	0.016	[24, 25]
Closed interior double door	0.027	[24, 25]
Open elevator door	2.0	–
Closed elevator door	0.05	[15]

2.3. Flow Loss Coefficient

According to the ASHRAE Handbook [26], tests were carried out to evaluate the mass flow through door leakages (Fig. 3). The results were based on a pressure difference of 0.3 inch of water (about 74.8 Pa). We determined the flow loss coefficient ($K = 3.56$) and discharge coefficient ($C_D = 0.53$) were valid for crack widths of 0 to 0.3 inch. For exterior leakages in the building envelope, $C_D = 0.65$ was used, according to the ASHRAE Handbook [26].

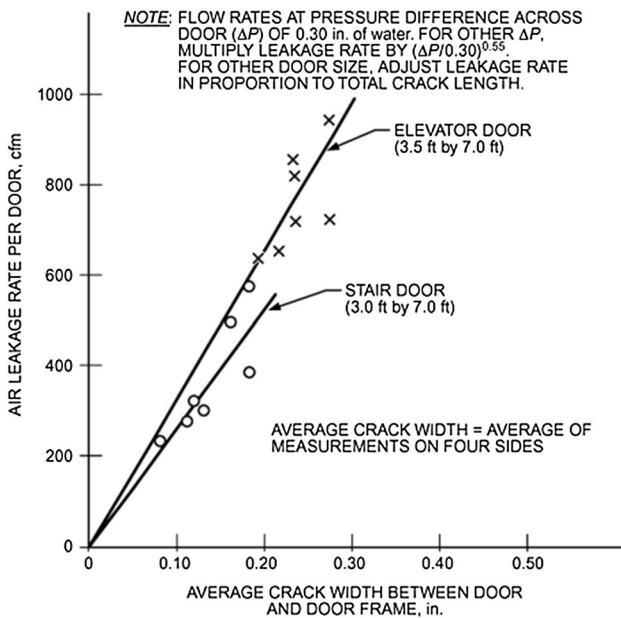


Figure 3. Mass flow rate varies with crack width (ASHRAE Handbook) [26].

2.4. Ventilation Conditions

In reality, the windows and doors of a building are either open or closed, which leads to different ventilation conditions. As discussed above, leakages or gaps exist even when the windows and doors are closed. According to the states of flow paths (closed/open), six typical ventilation conditions were considered (Table 2). Each case was named either “CS-X”, an abbreviation of the weather-induced stack effect, or “FS-X”, for the fire-induced stack effect, according to the causes of stack effect. In these scenarios, the elevator door of the fire/second level was considered to be either closed or open. Open elevator doors at this level significantly increase smoke flow into the shafts, which is one of the worst fire situations. The windows at the envelope are also considered to be closed or open.

3. Weather-Induced Stack Effect

During the heating season in winter, the warmer indoor air rises up, causing a reduction in pressure at the base of the building. This low pressure draws in cold air through the open windows and leakages. In other words, the difference between the indoor and outdoor air temperatures (or density) results in a stack effect within the building.

While investigating the weather-induced stack effect, the indoor air temperature is assumed to be uniform. This assumption is valid when the leakage area of the building is much smaller than the inner surface area. In this condition, the limited inflowing cold air is quickly heated by the air conditioning system. Based on this assumption, temperature and pressure distributions can be calculated theoretically. The impact of ventilation on the weather-induced stack effect was assessed as follows:

The typical flow paths and air temperatures of weather-induced cases are shown in Fig. 4. By way of simplification, the outside temperature was assumed to be 0°C (32°F) and the inside temperature 20°C (68°F), because of the heating system. It should be noted that the temperature difference could be larger or smaller depending on the local weather and air-conditioner setup.

Table 2
Summary of Ventilation Conditions

Case		Elevator door of fire/second level	Elevator door of other levels	Envelope of fire level	Envelope of other levels
Weather	Fire				
CS-1	FS-1	Leakage	Leakage	Leakage	Leakage
CS-2	FS-2	Leakage	Leakage	Open	Leakage
CS-3	FS-3	Leakage	Leakage	Open	Open
CS-4	FS-4	Open	Leakage	Leakage	Leakage
CS-5	FS-5	Open	Leakage	Open	Leakage
CS-6	FS-6	Open	Leakage	Open	Open

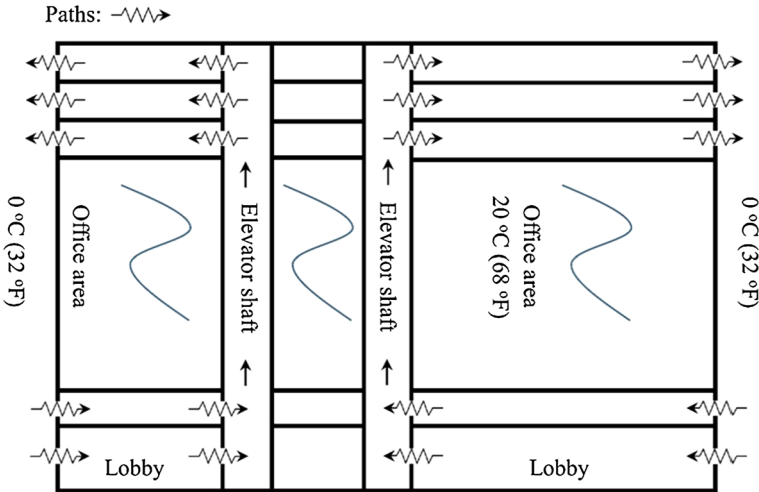


Figure 4. Flow paths and air temperatures for weather-induced cases.

In this situation, considering a total of 18 floors (80 m), the pressure difference within the building caused by the temperature difference could be simply calculated by Eq. (2).

$$\Delta P = K_s \left(\frac{1}{T_0} - \frac{1}{T_1} \right) h = 3460 \times \left(\frac{1}{273} - \frac{1}{293} \right) \times 80 = 69 \text{ Pa.} \tag{2}$$

Here, 69 Pa is the maximum pressure difference from top to bottom. To obtain the neutral plane height and the mass flow through these leakages, the detailed ventilation condition of the building must be specified. According to hydrostatic models, local pressure difference is a function of location and the density of the buoyant smoke plume:

$$\begin{cases} \Delta p(z) = \int_{h_{np}}^z (\rho_\infty - \rho_s) g dh \\ p|_{z=h_{np}} = 0 \end{cases} \tag{3}$$

where h_{np} is the neutral plane height (m) and ρ_∞ and ρ_s are the density of air and smoke. Based on the ideal gas state equation, the gas density is the function of gas temperature:

$$\rho = \left(\frac{P_{atm}}{RT} \right), \tag{4}$$

where P_{atm} is the atmospheric pressure (101,325 Pa) and R is the specific gas constant for air ($287 \text{ J kg}^{-1} \text{ K}^{-1}$).

The mass flow rate, \dot{m} , at the openings is a function of the pressure difference as:

$$\dot{m} = NC_D A \sqrt{2\rho\Delta p}. \tag{5}$$

where C_D is the discharge coefficient, A is the cross-area of the flow path, and N is a flow direction coefficient ($N = 1$, when $\Delta p > 0$; $N = -1$, when $\Delta p < 0$).

There are two flow resistant paths between the elevator shaft and outer space (the elevator doors and building envelope leakages) as shown in Fig. 5. Since there are in parallel eight elevator shafts in the building, the total flow area through elevator doors should be equal to eight times a single door's area. According to hydrostatic theory, the general flow resistance, $C_d A$, can be calculated using Eq. (6):

$$\frac{1}{C_d A} = \sqrt{\frac{1}{(8C_{d,e}A_e)^2} + \frac{1}{(C_{d,w}A_w)^2}}, \tag{6}$$

where A_e and A_w are the cross-area of the elevator doors and leakage on the building envelope, respectively, and $C_{d,e}$ and $C_{d,w}$ are the corresponding discharge coefficients.

As determined in Sect. 2.2, typically, the leakage area of a closed elevator door is about 0.05 m² and the exterior leakage area on the building envelope of a floor with normal height is about 0.12 m². The other leakage area refers to Table 1.

The discharge coefficient has been addressed in Sect. 2.3. Based on Eq. (6), for each case, the general flow resistance at lobby, second, and the other floors could be calculated. The calculation results are shown in Table 3.

Then, the mass flow rate at lobby, second, floor and upper floors can be expressed, respectively:

$$\dot{m}_{lobby} = (C_D A)_{lobby} \sqrt{2 \frac{P_{atm}}{RT_{\infty}} |\Delta p_{lobby}|}, \tag{7}$$

$$\dot{m}_{second} = (C_D A)_{second} \sqrt{2 \frac{P_{atm}}{RT_{second}} |\Delta p_{second}|}, \tag{8}$$

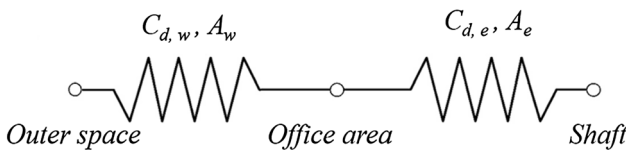


Figure 5. Combination of the flow resistance.

Table 3
Leakage Parameters and Calculated Neutral Plane Height Values

Case	General flow resistance C_{DA}/m^2			Neutral plane height h_{np}/m
	Fire floor	Lobby level	Other floors	
CS-1	0.07	0.16	0.07	41.7
CS-2	0.22	0.16	0.07	38.2
CS-3	0.22	0.22	0.22	43.9
CS-4	0.08	0.16	0.07	40.2
CS-5	12.78	0.16	0.07	13.3
CS-6	12.78	0.22	0.22	14.6

$$\dot{m}_{others} = \sum N(C_{DA})_i \sqrt{2 \frac{P_{atm}}{RT_i} |\Delta p_i|}. \quad (9)$$

Gas flow in and out an elevator shaft should further obey the mass conservation law. The mass conservation equation is:

$$\dot{m}_{lobby} + \dot{m}_{second} + \dot{m}_{others} = 0. \quad (10)$$

Substituting Eqs. (7)–(9) into Eq. 10., the neutral plane height could be solved. A program in Python language was used to solve the latter equation. The calculated neutral plane h_{np} is shown in Table 3.

Pressure differences among various ventilation conditions are shown in Fig. 6. These computed stack effect pressure differences are of similar magnitude to those reported by Jo et al. [8]. When the elevator doors and windows on the fire floor were all open, the neutral plane height was much lower compared with closed door/window cases.

In conclusion, the top–bottom pressure difference in an elevation shaft induced by weather only depends on the difference of exterior and interior air temperatures. In addition, the configurations of ventilation paths affect the height of the neutral pressure plane. Specifically, the general flow resistance (C_{dA}) of the floors connected to the elevator shafts determines the neutral pressure plane height in the weather-induced stack effect cases.

4. Fire-Induced Stack Effect

4.1. Mathematical Approach

When a fire outbreak occurs in a high-rise building, the heat released from the fire significantly raises the ambient temperature within the building, resulting in the fire-induced stack effect. In this situation, the interior air temperature is no longer uniform, which is quite different from the weather-induced stack effect. As a result, the corresponding physical prototype is much more complex. The CFD approach was used to assess the fire-induced stack effect in high-rise buildings.

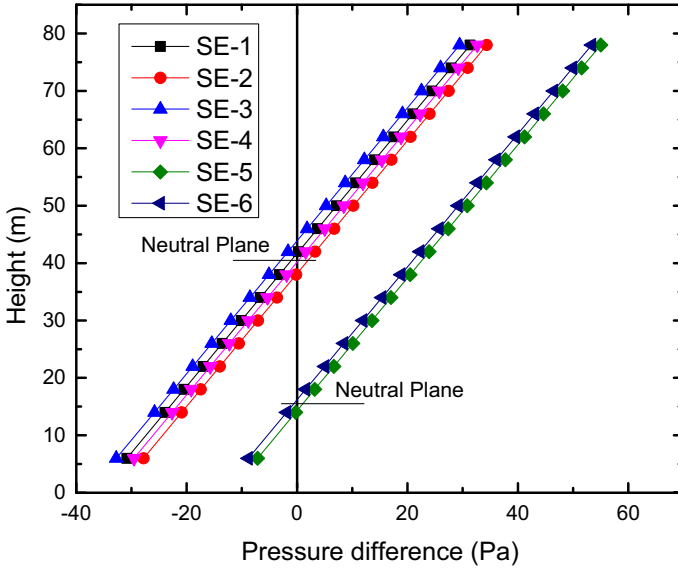


Figure 6. Pressure difference caused by stack effect (cold weather).

We used the Fire Dynamic Simulator program, which was developed by the National Institute of Standards and Technology, to perform CFD simulation. The program solves approximate forms of the Navier–Stokes equations [27, 28]. The equations for large-eddy simulation (LES) modeling of Navier–Stokes were derived by separating turbulent motions into large and small eddies using a filter. Therefore, any flow variable, $\varphi(x, t)$, can be decomposed by filtering it into a resolved large-scale component, $\varphi_L(x, t)$, and a sub-grid-scale component, $\varphi'(x, t)$, as shown below:

$$\varphi(x, t) = \varphi_L(x, t) + \varphi'(x, t). \tag{11}$$

The large-scale component was simulated directly, while small eddies were modelled by means of the Smagorinsky form of LES.

A mixing-limited infinitely fast reaction combustion model was used. The reactant species in any given grid cell were converted into product species at a rate determined by a characteristic mixing time. The heat release rate per unit volume was obtained by summing the products of all mass production rates of the species and the respective heats of formation:

$$\dot{q}''' = - \sum_{\alpha} \dot{m}_{\alpha}''' \Delta h_{f,\alpha}. \tag{12}$$

A duct flow model was designed to simulate air flow through small leakages, which is critical in flow calculation. Simple conservation equations of mass and energy combined with an implicit solver for the momentum conservation equation

based on the MELCOR solver were used [29]. Mass storage within the air transport route was not taken into account. The conservation equations of mass, energy, and momentum of the species (j) were as follows:

$$\sum_j \rho_j u_j A_j = 0, \quad (13)$$

$$\sum_j \rho_j u_j A_j h_j = 0, \quad (14)$$

$$\rho_j L \frac{du_j}{dt} = (p_{in} - p_{out}) + (\rho g \Delta z)_j - \frac{1}{2} K_j \rho_j |u_j| u_j, \quad (15)$$

where L is the length of the duct segment and K is the loss coefficient of the duct segment. The measured minor loss is usually given as a ratio of heat loss $h_m = \Delta p / (\rho g)$ through constriction to the velocity head $v^2 / (2g)$ of the associated piping system. Thus, the coefficient can be defined by Eq. (16):

$$K = \frac{h_m}{v^2 / (2g)} = \frac{\Delta p}{\frac{1}{2} \rho v^2}. \quad (16)$$

This minor loss coefficient is related to the discharge coefficient, C_d , via the following equation:

$$K = \frac{1}{C_d^2}. \quad (17)$$

4.2. Simulation Model

A 3-dimensional numerical model of the 18-story high-rise building was developed. Its structure and dimensions are described in Fig. 1. The main flow paths consisted of envelope leakages, door gaps, and elevator shafts; the eight elevator shafts inside the service core were the primary routes for vertical air flow.

It is significant that we used a duct flow model to simulate air circulation through small air flow paths, including the envelope leakages and elevator door gaps. Since the spatial scale of small leakages and gaps are too small compared to the huge size of a high-rise building, it is hardly possible to directly simulate air flow through the leakages and gaps with the large-scale air movements in the building at the same time. In order to fix this problem, the leakage and gap air flow were obtained separately using the empirical formulas described in Sect. 4.1. The CFD simulation mainly concentrated on building scale flow features, especially the fire-induced stack effect.

Based on the concept of separating the two air flow scales, there was no need to use tiny meshes to obtain the detailed flow field through the leakages and gaps in

the simulation model. Considering the large scales of the physical/computational domain (i.e., 70 m × 45 m × 72 m), a relatively coarse mesh size of 0.5 m was used. The total number of grid cells was 1,866,240. They were divided into eight meshes for parallel computing.

In high-rise buildings, due to the stack effect, fire is potentially more dangerous when occurring at lower levels. We considered the situation of fire taking place in the office area on the second floor above the lobby, since more combustible materials are found at this level than in the lobby. A full-scale fire test of a single office workstation was carried out by NIST as part of the 9/11 accident investigation [30]. The peak heat release rate (HRR) of a single workstation was about 7.0 MW, with a relative expanded uncertainty of approximately $\pm 15\%$. The t-squared fire model was adopted to describe the fire growth phase. Since furniture contains a lot of foam materials, the fast t-squared growth model was used for the early stage. A fast fire growth rate of $\alpha = 0.0469 \text{ kW/s}^2$ is suitable for this scenario. Thus, the calculated duration of the fire growth phase was 386 s. Figure 7 presents the HRR profile.

4.3. Smoke Spread in High-Rise Buildings

Typical smoke spread processes after ignition were observed from the simulations (Fig. 8). In the simulation models, the initial inside and outside temperatures of high-rise buildings are considered to be equal. As a result, no stack effect occurs in the beginning. As in common compartment fires, smoke generated from the fire first fills the local floor from the ceiling (Fig. 8a). When the smoke layer height reaches the elevator doors, hot gas starts to enter the elevator shafts. Due to buoyancy, hot gas generally rises in the shafts with less restriction (Fig. 8b). In this case, gas temperature inside the shafts significantly increases, and the stack effect starts to occur. Due to the pressure difference at the lower elevator doors,

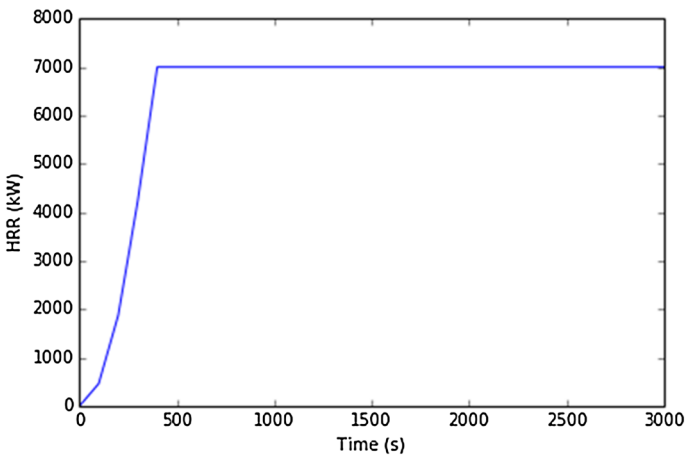


Figure 7. Heat release rate (HRR) of fire from a single office workstation.

fresh air would be drawn into shafts through the leakages, with hot smoke gradually filling the shafts. Finally, hot smoke arrives at the upper floors and flows out of the shafts through elevator doors, finally exhausting out of the building (Fig. 8c). Steady smoke movement throughout the high-rise building could then be observed from the simulation. There was a neutral plane around the middle height of the high rise. Above this neutral plane, smoke flows out of the shafts, while below it, gas flows into the shafts.

Temperature is a key feature in describing fire developments and flow characteristics. The temperature profiles of different heights in a shaft are presented in Fig. 9. Generally, the temperature development process could be divided into four stages. In stage (1), the temperature profile remains flat since the smoke is fully restricted under the ceiling of the fire floor, with no smoke entering the shafts until time t_1 . In stage (2), more and more smoke flows into the shafts, increasing the temperature at different height rises in sequence. The smoke front would finally reach the top of the shafts at time t_2 . Afterwards, the gas temperature in the shafts would continually increase before stability at t_3 . The temperature change between t_2 and t_3 is determined as stage (3), which precedes the final steady stage (4). The time point dividing the four stages in all six cases is marked in Fig. 9 as well. However, due to different ventilation conditions, the durations of various stages are different.

Key time points determined from the temperature profiles, i.e., t_1 , t_2 , and t_3 , of the six cases are summarized in Table 4. The t_1 values for the various cases were very close, all around 170 s. This is reasonable since t_1 could be considered the smoke filling time at the fire floor, which is mainly affected by the building geometry and fire size. In the simulation model, these two factors are unchanged in dif-

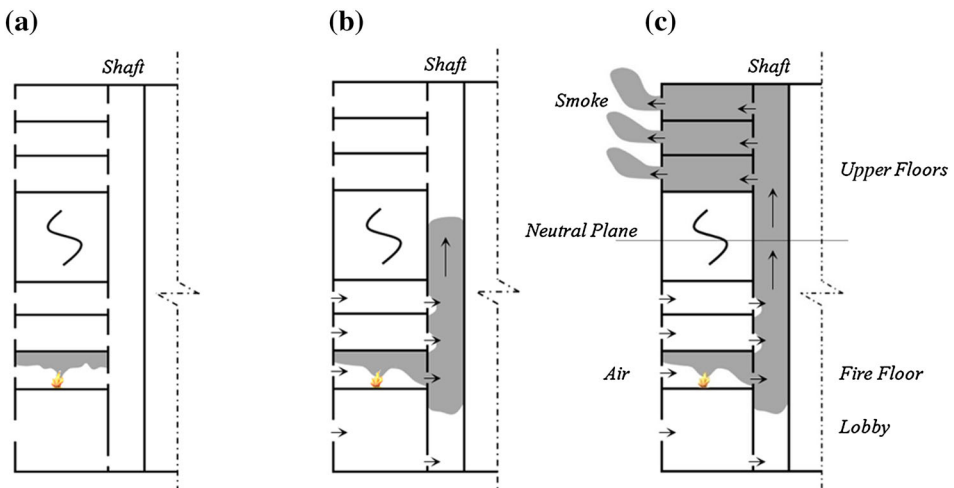


Figure 8. Smoke spread processes. (a) Smoke filling the fire floor, (b) smoke rising in shafts, (c) smoke flowing out of the building.

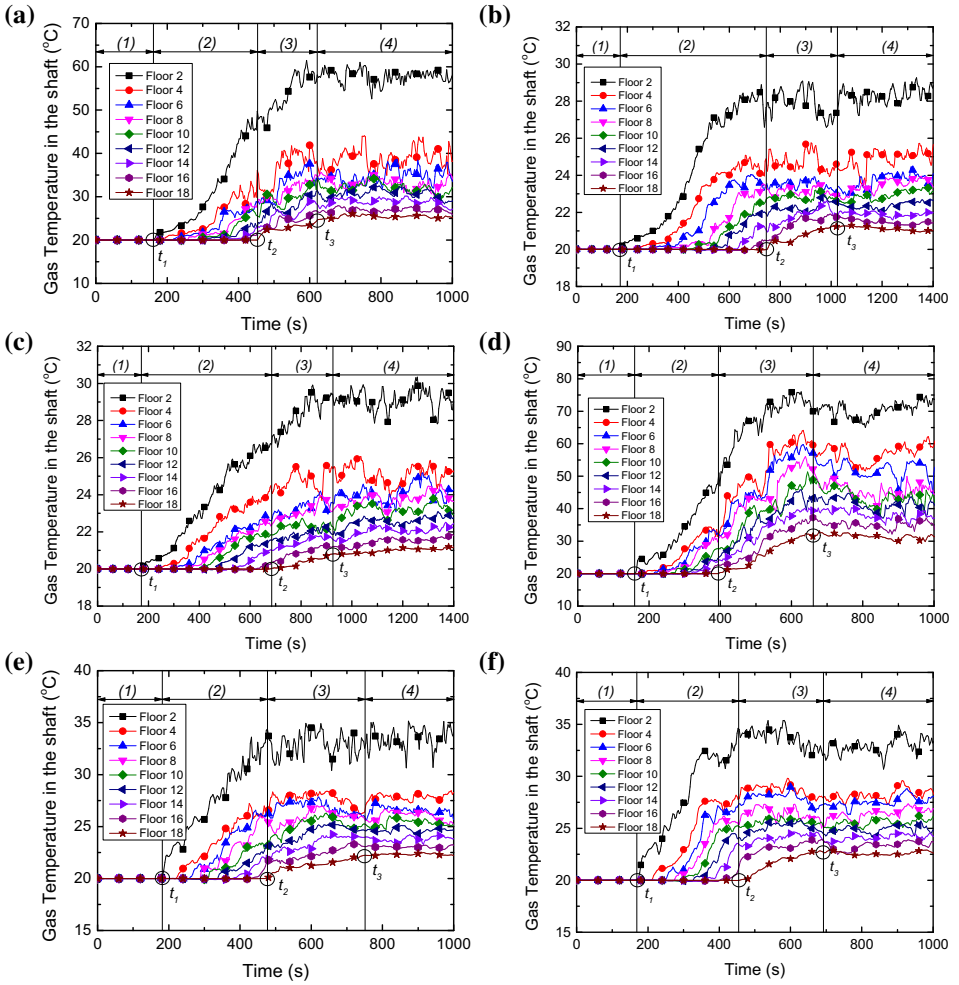


Figure 9. Temperature in the shaft under various ventilation conditions. (a) FS-1, (b) FS-2, (c) FS-3, (d) FS-4, (e) FS-5, (f) FS-6.

ferent cases. Unlike t_1 , t_2 , and t_3 vary a lot among cases. Indeed, both t_2 and t_3 of cases FS-2 and FS-3 were significantly larger than those of the remaining cases.

The smoke movement process in shafts could be further assessed from simulation results. While t_1 represents the time point at which smoke starts getting into elevator shafts, $t - t_1$ is the smoke traveling time after entering the shafts. Thus, the rise time of smoke from the fire layer in shafts, τ , could be defined by Eq. (18).

$$\tau = t - t_1 \tag{18}$$

Plume movement in shafts has been evaluated by Tanaka et al. [10]. In their study, the heat transfer from a fire plume to surrounding walls was insignificant.

Table 4
Key Time Points Determined from Temperature Profiles of Six Cases

Case	t_1/s	t_2/s	t_3/s
FS-1	162	453	621
FS-2	171	747	1026
FS-3	170	684	927
FS-4	159	396	660
FS-5	180	477	753
FS-6	168	456	693

Based on this assumption, the authors proposed an empirical model to express the relationship of rise time and rise height as follows:

$$\tau \propto A\dot{Q}^{1/3}z^{2/3}, \quad (19)$$

where τ is the travel time of a fire plume front from the source to a given height (s), \dot{Q} is the heat release rate (kW), A is the horizontal section area of the rising plume (m^2), and z is the distance from the fire source (m). Based on Eq. (19), the rise time is proportional to two thirds the power of the rising height for a certain fire size and section area. Ji et al. investigated the rising characteristics of fire-induced buoyant plumes in stairwells experimentally [13, 14] and found that the time for the buoyant plume front to reach a given height from a fire source is proportional to the 1.203 and 2.129 power of the height in a stairwell with the top vent open and closed, respectively. It should be noted that, compared with smoke movement in shafts, smoke plume movement in a stairwell was further affected by stairwell treads. Consequently, the upward movement was blocked.

In this study, the rise time of the smoke front was determined as proposed by Tanaka [10]. At a certain moment after ignition, the temperature profile at a given height would show a sudden temperature rise due to the contact of a rising plume, as shown in Fig. 9. Smoke rise time for all the six cases was plotted versus the vertical distance from the fire, $z \equiv h - h_{lobby}$ in logarithmic coordinates (Fig. 10). Fitting lines using Eq. (20) were plotted in the latter figure as well.

$$\tau = \alpha z^\beta \quad (20)$$

In this equation, the coefficients α and β reflect the plume rising speed in the shafts. According to Tanaka's analysis, the coefficient α is related to the heat source in the shaft, as $\alpha \sim \dot{Q}^{1/3}$. In this study, the fire was placed in the open office area, which is far away from the elevator shafts, and only part of the smoke flowed into the shafts. Although a fire with the same heat release rate in all the cases was used in the models, heat flowing into the shaft depended on the flow resistance at the fire floor. Therefore, the ventilation condition of the fire floor affected α significantly. From the fitting results in Fig. 10, the α values of FS1 and

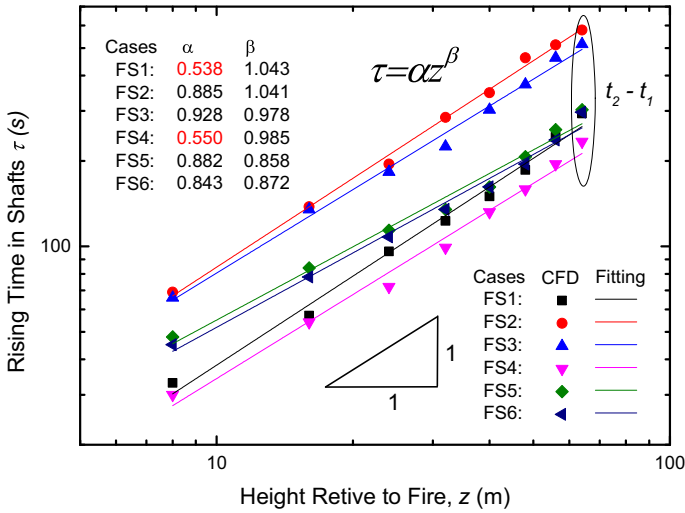


Figure 10. Smoke rise time versus the vertical distance from the fire in the six cases.

FS4 were significantly smaller than those of other cases. In these two particular cases, the envelope of the fire floor was nearly closed, which reduced smoke exhausting from the envelope. And as a result, more smoke entered the vertical shafts.

The coefficient β was around 1.0 in this study, which is slightly higher than Tanaka’s theory. In Tanaka’s study, the time for the buoyant plume front to reach a given height from a fire source was proportional to two thirds the power of the heat inputting rate when heat transfer from hot smoke to the shaft wall was insignificant. Considering the relative large dimensions of high rises and the large number of elevator door leakages along the shafts, both convective and conductive heat losses from the shaft wall could not be ignored. Heat loss from the shaft wall would significantly reduce the buoyancy driving force of the smoke plume. Thus, this decreased the smoke rise speed in the shafts.

In conclusion, the ventilation condition significantly affects the initial smoke plume movement throughout the building. The ventilation condition of the fire floor alters the gas flow rate into elevator shafts, while ventilation of the upper floors impacts the smoke rise speed in vertical shafts. These findings are useful in guiding the fire protection design in high-rise buildings. When a fire took place, opening the windows on the fire floor could be one of the efficient choices to delay smoke spread in a high-rise building.

4.4. Temperature and Pressure Distributions in Shafts

The temperature distribution within the elevator shafts is critical in determining the characteristics of the stack effect. As shown in Fig. 9, the temperature in the shaft reached steady state after a certain period of time (600–1000 s). In the

steady state, the temperature in the shaft decreased with height. Cooper [17] and Sun [11, 12] assumed that the only possible significant component of flow velocity is along the axis of the vertical shaft. Based on this assumption, from the basic conservation equations of mass and energy, and the ideal gas equation of state, Sun [11, 12] obtained a relationship between dimensionless temperature rise and dimensionless height as follows:

$$\theta(z) = ae^{-bz}, \quad (21)$$

where the dimensionless temperature rise θ is defined as:

$$\theta \equiv \frac{T - T_{\infty}}{T_{\infty}}, \quad (22)$$

where T is the gas temperature in the shaft (K) and T_{∞} is the environmental temperature (K). Adopting a similar definition of dimensionless temperature rise, the relationship between the dimensionless temperature rise in the shaft in the steady state and height relative to fire could be obtained (Fig. 11). In Fig. 11, the relationship between the two parameters was fitted by Eq. (21). The values of a , b and the related fitting coefficients in different simulation cases are listed in Table 5. For all six cases, the coefficient b was around 0.02. The correlation coefficients of all six cases were between 0.96 and 0.99, demonstrating that the gas temperature in the shaft under real fire conditions decreases exponentially with height. Equation (21) could be further used in assessing the intensity of the stack effect in elevator shafts of high rises.

Figure 11 also shows the effect of ventilation on gas temperature in the shaft. The temperature in the shafts was significantly decreased with only the windows on the envelope of the fire level open (FS-2) compared with all leakage cases (FS-1). This is because a lot of smoke flows out of the building from open windows, maintaining the smoke layer on the fire floor at a certain height. As a result, less smoke entered the shafts. When only the elevator doors on the fire floor were open (FS-4), the temperature in the shafts was significantly increased. This is because flow resistance at the elevator doors sharply reduces, leading to much more smoke entering the shafts. There were two simulation cases with a window opening in all the other levels (FS-3 and FS-6). Opening these windows slightly decreased flow resistance in the upper floors and slightly increased the temperature.

Figure 12 presents the typical pressure profiles of different ventilation conditions. The pressure difference in the shafts throughout the building height showed different characteristics under various ventilation conditions. When the window on the fire floor was open, the pressure difference was much smaller compared to the other cases. Additionally, when the fire level elevator doors were open, the pressure difference was much larger than in the remaining cases.

Another important feature of pressure profiles in Fig. 12 was the height of the neutral plane. The height of the neutral plane is also closely related to the ventilation conditions of a building, as shown in the assessment of the weather-induced

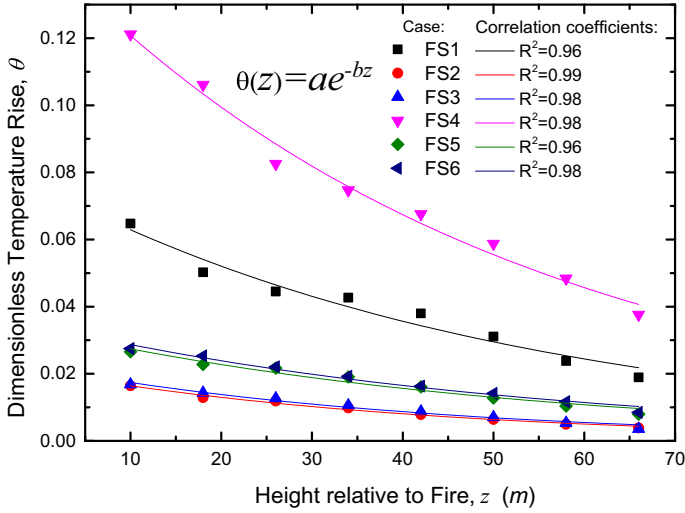


Figure 11. Dimensionless temperature rise in the shaft in the steady state for all cases.

Table 5 Parameters and Correlation Coefficients for Fitting in Fig. 11

Case	a	b	R ²
FS1	0.076	0.019	0.96
FS2	0.020	0.024	0.99
FS3	0.022	0.023	0.98
FS4	0.147	0.019	0.98
FS5	0.033	0.019	0.96
FS6	0.035	0.018	0.98

stack effect. In most cases, the height of the neutral plane was about half the height of the entire building, except for cases in which both the window and elevator doors on the fire floor were open. In these two cases (FS-5 and FS-6), the height of the neutral plane was significantly lower, in accordance with the situations in the weather-induced stack effect.

Overall, the impacts of ventilation on the fire-induced stack effect are more complex than those on the weather related stack effect. In the fire-induced stack effect, ventilation does not only affect the height of the neutral plane in a similar way to the weather-induced stack effect, but also influences the temperature in the shaft. In fire situations, opening the windows of the fire level could significantly decrease the shaft temperature and pressure difference, while opening elevator doors at the fire level might largely increase the shaft temperature and pressure difference. Opening windows on other floors has a limited impact on the stack effect, with only slightly increased shaft temperature and pressure difference.

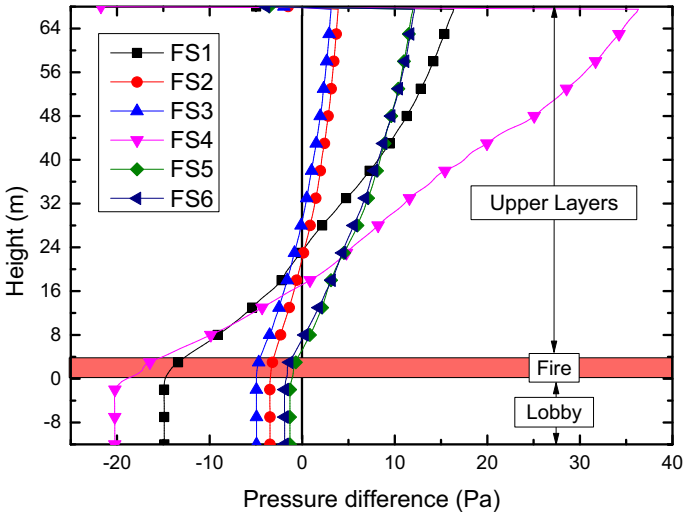


Figure 12. Effect of ventilation on pressure distribution in elevator shafts in the steady state.

4.5. Theoretical Model of the Fire-Induced Stack Effect

After assessing the characteristics of temperature and pressure distributions in elevator shafts, a theoretical model of the fire-induced stack effect in typical high rises was presented. Based on temperature distribution in the shaft, the pressure difference throughout the building could be calculated. While uniform temperature distribution was assumed in characterizing the weather-induced stack effect, the vertical temperature distribution in real fire scenarios in the steady state was found to decrease exponentially with height as in Eq. (21). In a previous study of the stack effect in elevator shafts, heat loss from the shaft wall was assumed to be insignificant, and the temperature in the shaft was considered to be uniform. However, in this work, both convective and conductive heat losses could not be ignored. Thus, the gas temperature in shafts should be obtained as:

Table 6 Comparison of Neutral Plane Heights Between CFD Results and Theoretical Calculation

Case	Neutral plane height determined from CFD results $h_{np,CFD}/m$	Neutral plane height calculated from model $h_{np,theoretical}/m$
FS-1	35.2	36.2
FS-2	34.1	35.0
FS-3	41.0	41.4
FS-4	29.3	31.7
FS-5	17.3	16.2
FS-6	19.3	16.8

$$T(z) = T_{\infty} + T_{\infty}\theta(z). \tag{23}$$

This is using the same models shown in the calculation of weather-induced stack effect. Substituting Eqs. (23) and (4) into Eq. (3), the difference in pressures between the inside and outside of the shaft at the typical three types of floors could be calculated after integration as:

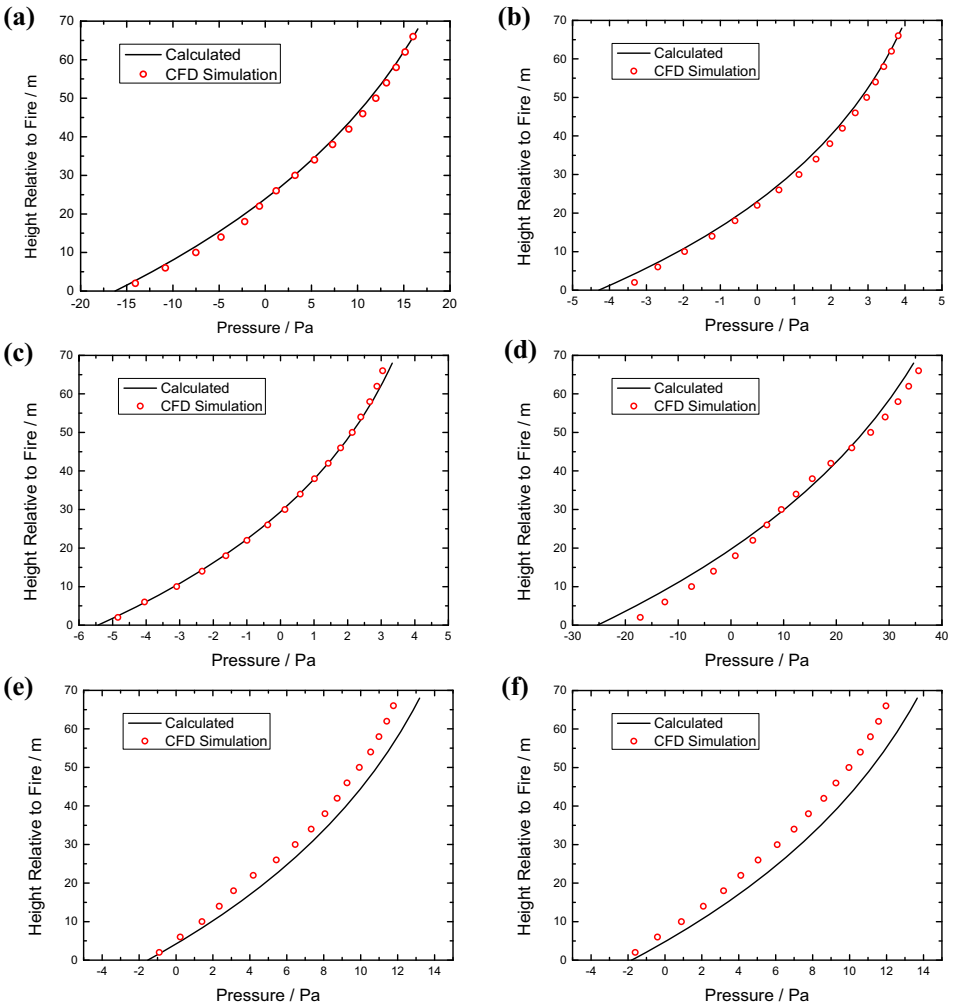


Figure 13. Validation of pressure difference calculated from the theoretical model using CFD results (a) FS-1, (b) FS-2, (c) FS-3, (d) FS-4, (e) FS-5, (f) FS-6.

$$\Delta p_{lobby} = -\frac{3463}{T_{\infty} b} \ln \frac{1+a}{1+ae^{-bh_n}}, \quad (24)$$

$$\Delta p_{fire} = -\frac{3463}{T_{\infty} b} \ln \frac{1+ae^{-bh_{fire}}}{1+ae^{-bh_n}}, \quad (25)$$

$$\Delta p_i = -\frac{3463}{T_{\infty} b} \ln \frac{1+ae^{-bh_i}}{1+ae^{-bh_n}}, \quad (26)$$

where Δp_{lobby} , Δp_{fire} , and Δp_i represent the pressure difference at lobby, fire floor, and i th floor (above fire floor) and h_{fire} and h_i are the elevation of fire floor and i th floor (above fire floor).

Substituting Eqs. (24)–(26) into Eqs. (7)–(9), the mass flow at each floor can be calculated. By applying mass conservation law as Eq. (10), the neutral plane height of the fire-induced stack effect can also be solved. Both the neutral plane height of the CFD result and the theoretical calculation are listed in Table 6. The neutral plane height calculated from the theoretical model in different ventilation conditions is generally in accordance with the CFD simulation results.

The pressure difference through high rises could then be calculated using Eq. (3). The pressure difference results from both CFD simulation and theoretical calculation for each case are plotted in Fig. 13, which shows that the model successfully predicted the pressure difference in high-rise buildings.

5. Conclusion

This work assessed the impacts of ventilation on both the weather- and fire-induced stack effects in an 18-layer high-rise office building by theoretical calculation and CFD simulation. The remarkable findings can be summarized as follows:

For the weather-induced stack effect, the ventilation condition of the building has a significant effect on the height of the neutral pressure plane, while the top to bottom pressure difference in a certain elevator shaft is only a function of the exterior and interior air temperatures.

The impacts of ventilation on the fire-induced stack effect are more complex than on the weather-induced stack effect. In real fire scenarios, smoke generated from the fire initially fills the fire floor after ignition. When the smoke layer descends to the elevator doors, hot smoke starts getting into the elevator shafts, significantly raising air temperature inside the elevator shafts. As a result, the hot air inside the elevator shafts, driven by the buoyancy force, flows vertically upward, causing the stack effect. Ventilation conditions affect the initial fire plume movement throughout the building significantly. The ventilation condition of the fire floor influences gas flow into elevator shafts, while that of the upper floors also impacts the smoke rise speed in vertical shafts. When the stack effect finally reaches steady state, the gas temperature in the shaft decreases exponentially with

height. In the steady state, the ventilation condition affects the neutral plane height in a similar way to the weather-induced stack effect, as well as shaft temperature.

A theoretical model of the fire-induced stack effect in typical high rises was presented. Based on the temperature distribution in the shaft, the pressure difference throughout the building could be calculated according to hydrostatic models and the mass conservation law. Results showed that the model successfully predicts the pressure distribution in high-rise buildings.

Acknowledgements

The authors would like to thank Prof. Ofodike A. Ezekoye from the University of Texas at Austin for the help with the discussion. The present work was supported by the National Key Research and Development Program of China (Project No. 2016YFC0800600), National Natural Science Foundation of China (Project No. 51706046), and the Science and Technology Commission of Shanghai Municipality (Project Nos. 13231201500 and 17YF1402800).

References

1. Jo J-H et al (2007) Characteristics of pressure distribution and solution to the problems caused by stack effect in high-rise residential buildings. *Build Environ* 42(1):263–277
2. Drysdale D (2011) *An introduction to fire dynamics*. Wiley, Chichester
3. Tamura GT, Wilson AG (1967) Pressure differences caused by chimney effect in three high buildings. *ASHRAE Trans* 73(2):11.1–10
4. Jo J-H, Yeo M-S, Yang I-H, Kim K-W (2004) Field measurement and evaluation of the impacts of the stack effect in high-rise buildings; case study. In: *Proceedings of the seventh international symposium on building and urban environmental engineering 2004*, pp 359–366
5. Tamblyn RT (1991) Coping with air pressure problems in tall buildings. *ASHRAE Trans* 97(1):824–827
6. Tamblyn RT (1993) HVAC system effects for tall buildings. *ASHRAE Trans* 99(2):789–792
7. Lovatt JE, Wilson AG (1994) Stack effect in tall buildings. *ASHRAE Transactions* 100(2):420–431
8. Jo J-H, Yeo M-S, Yang I-H, Kim K-W (2004) Solving the problems due to stack effect in tall buildings. In: *The CIB world building congress*
9. Cannon JB, Zukoski EE (1975) Turbulent mixing in vertical enclosures under conditions applicable to fires in high rise buildings, Technical Fire Report No. 1 to the National Science Foundation, California Institute of Technology, Pasadena, California, USA
10. Tanaka T, Fujita T, Yamaguchi J (1998) Investigation into rise time of Bouyant fire plume fronts. In: *Proceedings of the first international symposium on engineering performance-based fire codes*, Hong Kong, China, pp 220–228
11. Sun XQ (2009) *Studies on smoke movement and control in shafts and stairwell in high rise buildings*. A thesis for the doctor degree, State Key Laboratory of Fire Science, University of Science and Technology of China, Hefei, China

12. Sun XQ et al (2009) Studies on smoke movement in stairwell induced by an adjacent compartment fire. *Appl Therm Eng* 29(13):2757–2765
13. Ji J et al (2013) Experimental investigation on the rising characteristics of the fire-induced buoyant plume in stairwells. *Int J Heat Mass Transf* 64:193–201
14. Li LJ et al (2014) Experimental investigation on the characteristics of buoyant plume movement in a stairwell with multiple openings. *Energy Build* 68:108–120
15. Klote JH (2004) Hazards due to smoke migration through elevator shafts—volume I: analysis and discussion. technical report. National Fire Protection Research Foundation, Quincy, MA, Report 864-I
16. Black W (2009) Smoke movement in elevator shafts during a high-rise structural fire. *Fire Safety J* 44(2):168–182
17. Cooper LY (1998) Simulating smoke movement through long vertical shafts in zone-type compartment fire models. *Fire Safety J* 31(2):85–99
18. Miller Richard S, Beasley Don (2009) On stairwell and elevator shaft pressurization for smoke control in tall buildings. *Build Environ* 44(6):1306–1317
19. Jacques R (1996) Controlling stack pressure in high-rise buildings by compartmenting the building. Technical series. Vol. 97. Canada Mortgage and Housing Corporation (CMHC)
20. Koo SH, Jo JH, Seo HS, Yeo MS, Kim KW (2004) Influence of architectural elements on stack effect problems in tall residential building. CTBUH, October 10–13, Seoul, Korea
21. Utiskul Y et al (2005) Compartment fire phenomena under limited ventilation. *Fire Saf J* 40(4):367–390
22. Peatross MJ, Beyler CL (1997) Ventilation effects on compartment fire characterization. *Fire Saf Sci* 5:403–414
23. Cheung SCP et al (2006) The influence of gaps of fire-resisting doors on the smoke spread in a building fire. *Fire Saf J* 41(7):539–546
24. VanGeyn M (1994) Positive pressure furnace fire tests. Technical report. National Fire Protection Research Foundation, Quincy, MA, Report 6285
25. NFPA (2000) Recommended practice for smoke control systems, NFPA 92A. National Fire Protection Association, Quincy
26. Bagheri HM (2013) ASHRAE handbook, fundamentals
27. McGrattan K, Hostikka S, McDermott R et al (2014) Fire dynamics simulator, user's guide (version 6). National Institute of Standards and Technology, Gaithersburg, Maryland, USA
28. McGrattan K, Hostikka S, Floyd JE et al (2014) Fire dynamics simulator, technical reference (version 6), National Institute of Standards and Technology, Gaithersburg, Maryland, USA
29. Gaunt R et al (2000) MELCOR computer code manuals: reference manuals version 1.8.5, volume 2, Rev. 2. NUREG/CR-6119, US Nuclear Regulatory Commission, Washington, DC, 91
30. Ohlemiller TJ et al (2005) Fire tests of single office workstations. Federal building and fire safety investigation of the world trade center disaster (NIST NCSTAR 1-5C)